Differential superoxide production in phosphorylated neuronal nitric oxide synthase mu and alpha variants

Yadav Prasad Gyawali^{1, ‡}, Ting Jiang^{1, ‡}, Jing Yang², Huayu Zheng¹, Rui Liu¹, Haikun Zhang¹, Changjian Feng^{1,2}*

¹ College of Pharmacy, University of New Mexico, Albuquerque, NM 87131, USA

² Department of Chemistry and Chemical Biology, University of New Mexico, Albuquerque, NM 87131, USA

‡ Y. G and T.J contributed equally.

*Corresponding author. E-mail: <u>cfeng@unm.edu.</u> Tel: +1-505-925-4326.

Abstract

Neuronal nitric oxide synthase (nNOS) is regulated by phosphorylation in vivo, yet the underlying biochemical mechanisms remain unclear, primarily due to difficulty in obtaining milligram quantities of phosphorylated nNOS protein. The functional diversity of the nNOS isoform is also linked to its splice variants. Of note is that determination of phosphorylation stoichiometry remains as a challenge. This study first expanded a recent genetic code expansion approach to produce phosphorylated rat nNOSμ and nNOSα proteins through site-specific incorporation of phosphoserine (pSer) at residues 1446 and 1412, respectively. A quantitative mass spectrometric approach was then developed to analyze unphosphorylated peptides in phosphatase-treated and -untreated phospho-nNOS proteins. The observed pSer-incorporation efficiency consistently exceeded 80%, showing high pSer-incorporation efficiency. Notably, under L-Arginine-depleted conditions, pSer1412 nNOSα presented a significant reduction in superoxide generation, whereas pSer1446 nNOS exhibited the opposite effect, compared to their unphosphorylated counterparts. This suggests that phosphorylation at the C-terminal tail has a regulatory effect on NOS activity that may differ between variants and isoforms. Furthermore, the methodologies for incorporating pSer into large protein and quantifying the percentage of pSer should be applicable to other protein systems.

Keywords: nitric oxide synthase, phosphorylation, quantitative mass spectrometry, superoxide, EPR spin trapping

Abbreviations: NO, nitric oxide; NOS, NO synthase; nNOS, neuronal NOS; eNOS, endothelial NOS; iNOS, inducible NOS; CaM, calmodulin; pSer, phosphoserine; O2-•, superoxide; AR, autoregulatory insert within the FMN domain of nNOS/eNOS; CT, C-terminal tail; BMPO, 5-tert-butoxycarbonyl-5-methyl-1-pyrroline-N-oxide; DDA, data-dependent acquisition; PRM, parallel reaction monitoring.

Introduction

Mammalian NOS is a family of enzymes responsible for producing nitric oxide (NO) from L-arginine (L-Arg) [1, 2]. NO is a signaling molecule in various physiological processes, including neurotransmission, regulation of blood vessel tone, and immune response. There are three NOS isoforms: neuronal, endothelial and inducible NOS (nNOS, eNOS, and iNOS, respectively). The nNOS and eNOS enzymes are primarily activated by calmodulin (CaM) binding to a linker region connecting the FMN and heme domains. Regulation of NOS by CaM also involves several intrinsic control elements including an autoregulatory (AR) insert within the FMN subdomain and a C-terminal tail (CT) [3] (Figure 1). The AR insert does not exist in iNOS isoform, and the C-terminal tail differs among the NOS isoforms in its length and sequence [4].

While Ca²⁺/CaM binding is the primary means of activating NOS, phosphorylation further regulates NO biosynthesis *in vivo* in response to a wide variety of stimuli [5, 6]. Notably, CT plays a key role in modulating NOS activity through phosphorylation [7]. Dysregulation of NOS phosphorylation can contribute to neurodegenerative disorders and cardiovascular diseases among other health issues. Therefore, it is of current interest to elucidate the mechanisms of NOS regulation by phosphorylation at specific residues such as serine. The effect of phosphorylation on NOS activities has been extensively studied using purified phospho-proteins [8] and phosphomimetic mutants [9-13], but the molecular mechanisms remain unclear to date. The common method of using aspartate or glutamate substitution to mimic the negative charge associated with phosphorylation presents limitations [14], and interpretations of observed mutational effects are indeed often controversial [12]. It is crucial to provide milligrams quantities of "native" phosphorylated NOS proteins for detailed structural and spectroscopic studies. However, it is impractical to isolate adequate amounts of phosphorylated NOSs from cells or tissues due to low *in vivo* levels and dynamic nature of phosphorylation modifications. To address this, we have utilized a recent genetic code expansion approach [15] to site-

specifically introduce phosphoserine (pSer), an unnatural amino acid, into rat $nNOS\alpha$ holoenzyme [14].

Besides CaM and phosphorylation, nNOS can undergo regulation by its splice variants, which represent distinct nNOS forms produced via alternative splicing of its mRNA [16]. One of the most studied nNOS variants is nNOSα, a muscle-specific nNOS, which is primarily found in skeletal and cardiac muscle cells. In comparison to nNOSα, nNOSα contains 34 additional amino acids in the AR region [17]. Despite the 34-residue disparity, nNOSα and nNOSα generally exhibited similar spectral characteristics, substrate and CaM binding affinities, as well as NO synthesis activity when L-Arg substrate level was adequate [18]. It is important to note that the nNOSα isoform does display distinctive characteristics in superoxide (O2•) production under L-Arg substrate depletion conditions: uncoupled nNOSα generates significantly lower levels of O2• in comparison to nNOSα [19, 20].

In this study, our focus is on investigating phosphorylation at a serine residue of the CT region (S1412 and S1446 in nNOSα and nNOSα, respectively), as its functional significance has been well established *in vivo* [21, 22]. We have extended the genetic code expansion method from nNOSα [14, 15] to the nNOSα variant for site-specific incorporation of pSer. The generation of pSer-incorporated recombinant nNOS protein requires a toolkit that contains a pSer orthogonal translational system (OTS), an expression plasmid encoding the nNOS protein, and an appropriate bacterial host strain for protein production. We have optimized the phosphonNOS preparation protocol, in which Sep-OTSλ, pCRT7 NT Topo vector and C321. □A □SerB strain were used for site-specific pSer-incorporation guided by TAG codon [15]. Significantly, we have established a LC-MS/MS approach to assess pSer-incorporation efficiency in the recombinant nNOS proteins. Additionally, via EPR spin trapping experiments, we have obtained

new direct evidence that demonstrates the distinct effect of phosphorylation on $O_2^{\bullet \bullet}$ production by the nNOS α and nNOS α variants.

Materials and Methods

Construction of expression plasmid. The wild type, unphosphorylated, rat nNOS expression plasmid (pJH-rnNOS∞) was created through circular overlap extension PCR. "Unphosphorylated" and "wild type" are used interchangeably in this work. The backbone PCR product was derived from plasmid pCRT7 NT Topo tetR/pLtetO Amp-wt sfGFP (Addgene #52053) [15], while the nNOS∞ gene was amplified from a nNOS plasmid [18]. These two fragments were fused together by circularizing them via overlapping sequences. Subsequently, the S1446TAG-nNOSµ expression plasmid (pJH-rnNOS∝ S1446TAG) was constructed through site-directed mutagenesis using combined overlap extension PCR; the primers are listed in Table S1 in Supporting Information. The plasmid map is depicted in Figure S1.

pSer1446 nNOS∞ protein overexpression and purification. The protein was overexpressed in C321.□A □SerB cells [15], a specialized *E. coli* strain for pSer-incorporation. The cells were transfected with the pJH-rnNOS∞ S1446TAG and SepOTSλ plasmids [14]. Due to the potential SepOTSλ instability, it is crucial to perform a step of re-streaking phosphoprotein expression strains from glycerol stocks onto fresh LB agar selection plates. This serves several purposes, including the evaluation of strain viability (e.g., assessing colony growth rate and uniform colony size) and the identification and exclusion of cells carrying mutant SepOTSλ constructs, which typically produce sporadic, larger colonies [23]. By implementing the practice, we have improved the reproducibility of recombinant phospho-nNOS generation.

Additionally, the unphosphorylated nNOS∞ was overexpressed in C321.□A cells with only the wild type pJH-rnNOS∞ plasmid and subsequently purified following the procedure [14].

NOS enzymatic activity assays. The steady state NO production rate was determined in a pH 7.4 buffer comprising 50 mM Tris, 100 mM NaCl, 5 μM tetrahydrobiopterin(H₄B), and 200 μM CaCl₂, as previously described [24]. The reaction mixture contained 100 μM L-Arg, 100 μM NADPH, 8 μM oxyhemoglobin, and 1 αM CaM. The reaction was initiated by adding nNOS protein to a final concentration of 20 nM and monitored at 401 nm for 2 minutes; the rate of NO synthesis was calculated using an extinction coefficient of 60 mM⁻¹ cm⁻¹ [24].

The oxidation of NADPH by nNOS was observed separately at 340 nm under identical buffer and final nNOS concentration conditions, but without oxyhemoglobin. To study the effect of agmatine on NADPH oxidation rate, 2 mM agmatine was present in the same assay mixture; the reaction was initiated by adding nNOS protein to a final concentration of 10 nM. The final nNOS concentration was reduced because of a faster NADPH oxidation rate in the presence of agmatine, compared to when this compound was absent. This is to yield a linear decay within 1 minute without curving too soon so that reliable initial velocity value can be achieved. The oxidation rate of NADPH was determined using an extinction coefficient of 6.2 mM⁻¹ cm⁻¹ [24]. Determination of pSer-incorporation efficiency by LC-MS/MS. A portion of the purified pSerincorporated nNOS protein sample was divided into two equal aliquots. One aliquot was subjected to dephosphorylation by Lambda Protein Phosphatase (New England Biolabs Inc.) with overnight incubation at 30 °C and continuous shaking at 100 rpm. The other aliquot was preserved at -20 °C after adding the same reaction buffer, but without the phosphatase. Both aliquots were subsequently digested using MS-grade Trypsin-LysC protease enzyme (Promega) in a 10 kDa cut-off MWCO filter device (Amicon Ultra-0.5); see Supporting Information for details. The sample preparations were conducted in triplicate.

LC-MS/MS analysis was then conducted on a Q Exactive Classic Orbitrap mass spectrometer (Thermo Scientific, San Jose, CA) equipped with an EasySpray ion source. Data-dependent acquisition (DDA) experiment was first performed to build the targeted peptide list. For parallel reaction monitoring (PRM) experiments, the targeted peptides inclusion list and Skyline (MacCoss Lab Software) PRM transition library were built by selecting all unphosphorylated peptide sequences containing the site of phosphorylated-serine in their phosphorylated peptide counterparts from the DDA experiment. Additionally, six peptides from the nNOS protein were incorporated as internal reference peptides for normalization purpose, namely, ANNSLISNDR, LQVFDAR, ATILYATETGK, DTELIYGAK, STIFVR, VTQPLGPPTK (referred to as N1 through N6, respectively, in Tables S2 and S4). These internal reference peptides were selected based on the following criteria: 1) sequence not next to the interested phosphorylation site; 2) no miscleavaged form detected in LC-MS/MS experiment; 3) relatively high abundance; 4) no possible modification such as oxidation (i.e., no methionine), carbamidomethylation (i.e., no cysteine), etc.; and 5) the sequences of all internal reference peptides cover a broad range of the nNOS protein sequence, rather than focusing on just the N-terminal, or just C-terminal, or in the middle part of nNOS only. For quantitative data analysis, raw PRM data files and a PRM transition library for PRM experiments were entered into Skyline software. The pSer% was calculated from the PRM peak areas of unphosphorylated peptides containing the serine 1412 or 1446 site in the phosphatase-treated and untreated samples; the peak areas were normalized using internal peptide reference. Additional experimental details are provided in the Supporting Information, and representative pSer% calculations are included in Tables S2-S5.

Measurement of superoxide production by EPR spin trapping. O₂-• generation from the purified nNOS protein was monitored by EPR spin trapping [25]. The protein aliquots went through only one freeze-thaw cycle prior to the EPR experiments, to minimize the potential variation in protein activity. Briefly, O₂-• production was assessed using a spin-trap 5-tert-butoxycarbonyl-5-

methyl-1-pyrroline-N-oxide (BMPO), and the BMPO-•OOH adduct was observed through its EPR spectrum. The nNOS protein was first buffer exchanged into a pH 7.4, 50 mM Tris buffer containing 250 mM NaCl, 10% glycerol, 0.1 mM DTT, 0.1 mM EDTA to obtain L-Arg-free nNOS protein. The EPR sample in a pH 7.4 phosphate buffer (50 mM) contained 100 μM DTPA, 100 μM EDTA, 40 nM nNOS, 1 μM CaM, 40 mM BMPO, and 0.5 mM CaCl₂. The reaction was initiated by adding NADPH to a final concentration of 150 μM.

The entire 200 μ L sample was promptly transferred into a gas-permeable Teflon Sub-Lite-Wall® tubing (ID 0.025 \pm 0.001 inch, wall 0.002 \pm 0.001 inch; Zeus Industries, Raritan, NJ),; the tubing was pre-cut at desired length for the sample volume. The sample-filled tubing was folded four times, and inserted into a quartz EPR tube open at both ends. The Teflon tubing mimics a flat cell for obtaining EPR spectrum of aqueous solutions with high dielectric solvent. The tubing allows a minimal surface area for the sample in the magnetic field so that an EPR signal can be acquired with higher resolution. Without using the Teflon tubing, we would have to use a flat cell and flat cell attachment with the resonator, and clean/soak/dry the flat cell after each use or have multiple flat cells to use throughout experiments. The tubing setup allows for EPR measurement of different samples without tedious usage of the flat cell(s).

The EPR spectra were recorded at a 15-minute mark after mixing on a Bruker EleXsys E500 X-band (~9.8 Hz) EPR spectrometer (Bruker Biospin, Billerica, MA) at room temperature. The following experimental parameters were used for data acquisition: microwave frequency, 9.8 GHz; modulation frequency, 100 kHz; center magnetic field, 3509 G; scan range, 110 G; microwave power, 21 mW; modulation amplitude, 1.0 G; time constant, 10 ms. Hamiltonian parameters of the BMPO-*OOH adducts were determined by simulations using the SpinFit function within the Xepr software.

Determination of Fe and Zn levels in purified nNOS proteins. Iron and zinc contents in the proteins were measured by ICP-MS. The proteins were digested in a heat block using 70% trace metal-grade nitric acid (Aristar Plus grade, BDH). Samples were heated gradually (ramp and hold) to 95 °C and kept for 1 h. After digestion, the samples were diluted with 18 M-ohm water prior to ICP-MS analysis. The metal analysis data are listed in Table S6.

Results and Discussion

Generation and enzymatic activities of pSer1446 nNOS∞ holoprotein

The overexpression of pSer1446 nNOS∞ in *E. coli* C321.□A was accomplished with an average protein yield of 2.8 mg per liter of cells. The purity was determined by SDS-PAGE, Coomassie staining, and densiometric analysis to be at least 80-85% (Figure S2). Figure S3 displays absorption spectra of isolated pSer1446 nNOS∞ protein. Following treatment with L-Arg, the NOS heme site exists in the high spin state, evident from the Soret peak at 394 nm. Additional shoulders were observed at 450 and 480 nm, attributable to flavin absorption. The CO difference spectrum in Figure S3 inset demonstrates that the heme center is of the native thiolate-heme complex, with an absorption peak at 444 nm and no 420 nm band. These spectral data indicate the intactness of the cofactor- and substrate- binding sites, as well as their accessibility to L-Arg. ICP-MS analysis demonstrated that recombinant pSer1446 nNOS∞ protein was purified with ~ one iron (1.25 ± 0.22) and 0.5 zinc (0.48 ± 0.02) per subunit. This is expected for homodimeric nNOS containing 2 Fe and 1 Zn per protein. These data showed that the purified pSer1446 nNOS∞ protein bound Fe and Zn stoichiometrically. The other nNOS proteins contained similar levels of these essential metal cofactors (c.f. Table S6).

To assess the enzymatic activities of the isolated proteins, we measured their steady state NO production and NADPH oxidation rates (Table 1). The NO synthesis rate (57.2 \pm 2.8 min⁻¹)

observed for unphosphorylated nNOS ∞ expressed in *E. coli* C321. \square A is within the range of previously reported values [24]. Moreover, an unpaired *t*-test comparing the average rates of NO production between unphosphorylated and pSer1446 nNOS ∞ proteins gave a two-tailed P-value of 0.1820. By conventional standards, this difference is not statistically significant.

Moreover, when unphosphorylated and pSer1446 nNOS α proteins were saturated with L-Arg, they exhibited NADPH/NO ratios of 2.14 ± 0.07 and 2.06 ± 0.06 , respectively (Table 1). A two-tailed *t*-test returned a P-value of 0.2073, indicating no significant statistical difference. Notably, pSer1412 nNOS α exhibit similar NADPH/NO ratio as well, comparing to its unphosphorylated form (Table 1). These data suggest that there is no discernible distinction in the degree of coupling between the phosphorylated and unphosphorylated nNOS proteins under L-Arg-repleted conditions. In fully coupled conditions, NOS necessitates 1.5 NADPH molecules for each NO molecule produced. Deviations from this ideal ratio imply the generation of reactive oxygen species at the expense of NO production.

Phosphorylation stoichiometry of the pSer-incorporated nNOS proteins

The site-specific pSer incorporation at 1446 of rat nNOS∞ was confirmed by MS/MS analysis (Figure S4). It is crucial to further ensure and validate high pSer-incorporation efficiency into NOS. Phosphorylation stoichiometry determination by LC-MS/MS is the preferred method due to its sensitivity, precision, and reliability. However, such measurement remains as a challenge [26], due to multiple issues including different ionization efficiency of phosphopeptides, and impaired proteolytic cleavage near phosphorylation site that often results in multiple phosphorylated peptides with miscleavages. Indeed, in our LC-MS/MS analysis, we detected four peptides containing the pSer1446 residue: SESIAFIEESK, SESIAFIEESKK, LRSESIAFIEESK, and LRSESIAFIEESKK. This makes absolute quantitation with isotopelabeled authentic standards prohibitively expensive and impractical.

We have tailored a label-free relative quantitation approach by PRM [27], where the pSer% quantitation relies on identifying and measuring the levels of each unphosphorylated peptide with and without phosphatase treatment (Figure 2). Because only unphosphorylated peptides are measured by LC-MS/MS, the challenges related to impaired ionization efficiencies and typically poor MS/MS spectra of phosphopeptides are bypassed. The problem that arises from impaired proteolytic cleavages in proximity of phosphopeptides during protein digestion is also minimized. The phosphorylation stoichiometry was determined by evaluating the abundances of unphosphorylated Ser-containing peptides in the two distinctively treated samples, with normalization achieved using the internal peptide references. Subsequently, the pSer% values were averaged across the four Ser1446-containing peptides. The experiments were replicated at least three times for different batches of purified pSer1446 nNOSα and pSer1412 nNOSα proteins. Notably, the measured pSer% consistently exceeds 80 % for the phosphorylated nNOS proteins prepared in different weeks.

Comparing superoxide production properties of the pSer-incorporated nNOS proteins

NOS uncoupling is a commonly observed phenomenon where the enzyme produces $O_2^{\bullet \bullet}$ instead of NO or in addition to NO. This can be caused by deficiency in its L-Arg substrate or H₄B cofactor. Unlike eNOS, nNOS predominantly exhibits uncoupling when lacking L-Arg, instead of H₄B [28, 29]. We thus assessed $O_2^{\bullet \bullet}$ production by the nNOS protein under various L-Arg concentrations. In all tested samples, saturated CaM (1 α M) was present along with nNOS, as $O_2^{\bullet \bullet}$ generation from nNOS protein occurs primarily at the heme site [30], and CaM is essential for facilitating electron transport across the NOS domains to reduce the heme center, which is required for O_2 binding to the Fe(II) center and subsequent $O_2^{\bullet \bullet}$ formation.

Using EPR spin trapping method [25], we quantified O₂• generation from the pSer-incorporated nNOS protein, in comparison to its unphosphorylated counterpart. High-purity (>

99%) BMPO was used as the spin trap. The EPR spectra of all the BMPO- $^{\bullet}$ OOH adducts can be simulated with a g value of 2.006 and hyperfine coupling constants of $A_N = 13.4$ G, $A_H^{\beta} = 11.8$ G for conformer I, and $A_N=13.3$ G, $A_H^{\beta} = 9.5$ G for conformer II. These results are consistent with previous reports [25, 31]. An example of EPR simulation is depicted in Figure S5.

All nNOS proteins in this study were overexpressed in C321. Δ cells, while nNOS proteins in most of the literature, including our previous study [25], were prepared using BL21 DE3 cells. It is thus necessary to examine the O2* generation property of the wild type nNOS protein purified from C321. Δ cells. In the absence of L-Arg, unphosphorylated nNOSα and nNOSα proteins both produced O2*, and nNOSα produced a substantially higher level of O2* compared to nNOSα (Figure 3). These results are consistent with prior reports on O2* production by recombinant nNOSα and nNOSα proteins prepared in DE3 cells [19]. Moreover, the adduct signal of nNOSα was significantly suppressed by the addition of 100 αM L-Arg (Figure S6); this concentration is physiologically relevant and well above the Km value of L-Arg (2 μM) [32]. The unphosphorylated nNOSα protein exhibited a similar dependence on L-Arg for its O2* production (Figure S6). These observations align with previous reports on L-Arg-dependent O2* production by nNOS [19]. The wild type nNOS proteins overexpressed in C321. Δ cells thus exhibit similar behavior in O2* production as those nNOS proteins obtained from BL21 DE3 cells.

We then measured the level of O₂•- production by the phospho-nNOS proteins. A comparison of EPR peaks at specific time offers a good differential comparison between the proteins. Measuring the relative peak heights in EPR spectra of the BMPO-•OOH adduct is a well-established method for comparing O₂•- free radical production across samples under identical experimental conditions. These conditions include using the same final nNOS concentration,

total sample volume within the EPR cavity, and EPR instrument settings. It is well accepted in the field to present changes in EPR intensity/height as a representative quantitative measurement of trapped radical, particularly $O_2^{\bullet -}$, as other methods such as ferricytochrome c assay has shown complications with the NOS system [33].

Notably, in the absence of L-Arg, pSer1446 nNOS α exhibited significantly higher $O_2^{\bullet-}$ level, whereas pSer1412 nNOS α displayed considerably lower $O_2^{\bullet-}$ production, in comparison to their unphosphorylated counterpart (Figure 3). Figure S6 shows the comparison of relative EPR intensity for the BMPO- $^{\bullet}$ OOH adduct; the relative height of the first EPR peak at the low magnetic field is determined by measuring from the peak to the zero line. We observed a relative height of 0.136 ± 0.030 for unphosphorylated nNOS α , which increased to 0.220 ± 0.001 for pSer1446 nNOS α . These values were found to be statistically different according to an unpaired t-test, giving a two-tailed p-value of 0.0084. Of note is that zinc or iron content variation is not the reason for the difference in $O_2^{\bullet-}$ production: there were plenty of zinc and iron present in the purified nNOS proteins as assessed by ICP-MS analysis (Table S6).

How $O_2^{\bullet-}$ production is modulated by the phosphorylation differently is an intriguing biochemical question. There is strong evidence that $O_2^{\bullet-}$ generation in nNOS is primarily through the heme site and can be significantly reduced by L-Arg (Figure S6) [25, 28, 34]. For example, it was estimated that only $\sim 10\%$ $O_2^{\bullet-}$ was produced at its reductase domain [34]. The notable differences in $O_2^{\bullet-}$ production between nNOS α and nNOS α are thus unlikely due to variation in the heme versus the reductase ratios of $O_2^{\bullet-}$ generation. We considered using diphenyliodonium (DPI), a flavoprotein inhibitor, to probe $O_2^{\bullet-}$ production from the reductase domain [28, 35]. It is important to note that the reported inhibitory effect of DPI cannot definitively establish whether $O_2^{\bullet-}$ is produced solely at the reductase domain [28], nor clearly discern the ratio of $O_2^{\bullet-}$

production between the reductase and heme domains. This complexity arises from the fact that the DPI-inhibited flavin domain not only exhibits reduced capacity in transferring electrons to dioxygen, but also is less efficient in transferring electrons to the heme domain, and as a result, the $O_2^{\bullet-}$ production in the heme site can also be inhibited. Therefore, the DPI experiment would be ambiguous to distinguish the ratio of $O_2^{\bullet-}$ production between the two domains.

We next considered if difference in heme reduction rates can explain the observed effects, as O₂• is generated mainly in the heme site. To test this, we measured NADPH oxidation rate in the presence of 2 mM L-agmatine, an inactive substrate analog [36]. The NADPH oxidation rate with added L-agmatine reports the steady state electron flux through the nNOS heme to O₂ in the CaM-bound nNOS, which is proportional to the rate of heme reduction under the same conditions [37]. We found that the NADPH oxidation rates in the presence of L-agmatine generally correlate with the O2[•] production in the phosphorylated nNOS proteins vs. their unphosphorylated forms: pSer1412 nNOSα exhibits lower rate than wild type nNOSα, while pSer1446 nNOS∞ has faster NADPH oxidation than wild type nNOS∞ (Table S7). This is consistent with the opposite effect observed in O2°- production. We are aware that the heme reduction rate of pSer1446 nNOSα is slower than that of pSer1412 nNOSα, while pSer1446 nNOS∞ makes slightly more O₂•- than pSer1412 nNOSα. This implies that in addition to heme reduction, other factors such as conformational states may contribute to O₂• generation as well. The notion of a pro-O₂•-conformation within NOS has been a subject of longstanding speculation in the literature [33, 38, 39].

Notably, the sole difference in the amino acid sequences of the two nNOS variants is in the additional 34-residue segment within the AR region of nNOS∞, whereas the phosphorylation events take place at the CT site, which is located distantly from the AR region (Figure 1) [40, 41]. Prior research has suggested that the AR and CT control elements may work synergistically

to modulate the conformational states of the nNOSα reductase domain [42]. In the context of the available structural data for nNOS catalysis, the insertion in the nNOSα AR region is also in a position consistent with the proposed interaction between AR and CT. As such, we speculate that phosphorylation at the CT site of nNOSα may induce distinct allosteric conformational changes, as opposed to nNOSα. These changes could account for the observed differences in O2⁻ production. Dynamic interplay among phosphorylation, conformational alterations, and O2⁻ production is a crucial pathway for regulating protein functions in general. For example, in immune cells, the activation of NADPH oxidases through phosphorylation triggers conformational changes that facilitate O2⁻ production [43].

The contrasting effects of phosphorylation at the same serine residue on the uncoupling of nNOSα and nNOSα may have potential biological implications. These results should be applicable to pathological conditions in which nNOS is uncoupled. In addition to NO production, nNOS generates O₂•, which plays important roles in both cell injury [44] and redox signaling [19]. For instance, in the context of cerebral ischemia, phospho-nNOS at Ser1412 significantly increased between 1 and 6 hours after reperfusion in the hippocampus [22], suggesting a potential contribution of nNOS phosphorylation at Ser1412 to injury. Our observation of reduced O₂• production by pSer1412 nNOSα might seem contradictory to the increased phospho-protein levels observed in the *in vivo* study [22]. However, it's important to note that the previous *in vivo* study did not directly assess O2 or nor NO levels, and the underlying mechanism could involve multiple factors, including formation of peroxynitrite and/or hydrogen peroxide, cellular localization of nNOS, feedback signaling, etc. [45]. In the NOS field, the prevailing perspective suggests that whether nNOSa is phosphorylated or not might not significantly impact its uncoupling. nNOSα phosphorylation is often regarded as a secondary occurrence, while the phosphorylation of nNOS∞ is considered more crucial. Further investigation is warranted to

better understand the functional implications of phosphorylated nNOSα and nNOS∞ variants.

In conclusion, we have expanded our recent pSer-incorporation approach and generated milligrams quantities of active pSer1446 nNOS^α protein. Additionally, we have established a tailored quantitative mass spectrometry protocol for assessing the extent of site-specific phosphorylation in the pSer-incorporated proteins. Notably, the measured pSer percentage consistently exceeded 80%, affirming the efficiency of pSer incorporation into the nNOS proteins. Furthermore, it is important to note that the phosphorylation exhibited opposite effect on O2^{*-} production by the nNOSα and nNOS^α variants. These findings should inspire detailed mechanistic investigation of NOS isoform regulation through phosphorylation using recombinant proteins with site-specific pSer incorporation.

Supporting Information. Experimental procedures in expression plasmid construction; LC-MS/MS sample preparation and PRM data collection; representative calculations of pSer% for individual peptide and the protein; SDS PAGE of purified nNOS proteins; example absorption spectra of the purified nNOS protein; simulation of EPR spectra of the BMPO-OOH adduct produced by the nNOS proteins; effect of L-Arg on the BMPO-OOH adduct signals.

Acknowledgements

This work is funded by NIH GM133973 and NSF 2041692 (C.F.). This material is also based upon work supported in part by NIH P20GM130422 and P30ES032755. We thank Dr. John Weaver for helpful discussions.

References

- [1] D.J. Stuehr, M.M. Haque, Br J Pharmacol 176 (2019) 177-188.
- [2] J. Li, H. Zheng, C. Feng, Frontiers in Bioscience-Landmark 23 (2018) 1803-1821.
- [3] T.L. Poulos, Chem. Rev. 114 (2014) 3919-3962.
- [4] M. Jachymova, P. Martasek, S. Panda, L.J. Roman, M. Panda, T.M. Shea, Y. Ishimura, J.J.P. Kim, B.S.S. Masters, Proc Natl Acad Sci U S A 102 (2005) 15833-15838.
- [5] D.J.R. Fulton, in: A.K. Raouf (Ed.), Adv Pharmacol, vol. Volume 77, Academic Press, 2016, pp. 29-64.
- [6] D. Fulton, J.P. Gratton, T.J. McCabe, J. Fontana, Y. Fujio, K. Walsh, T.F. Franke, A. Papapetropoulos, W.C. Sessa, Nature 399 (1999) 597-601.
- [7] K. Hinchee-Rodriguez, N. Garg, P. Venkatakrishnan, M.G. Roman, M.L. Adamo, B.S. Masters, L.J. Roman, Biochem. Biophys. Res. Commun. 435 (2013) 501-505.
- [8] C.A. Chen, L.J. Druhan, S. Varadharaj, Y.R. Chen, J.L. Zweier, J. Biol. Chem. 283 (2008) 27038-27047.
- [9] S. Adak, J. Santolini, S. Tikunova, Q. Wang, J.D. Johnson, D.J. Stuehr, J. Biol. Chem. 276 (2001) 1244-1252.
- [10] Q.M. Hanson, J.R. Carley, T.J. Gilbreath, B.C. Smith, E.S. Underbakke, J. Mol. Biol. 430 (2018) 935-947.
- [11] M.M. Haque, S.S. Ray, D.J. Stuehr, J. Biol. Chem. 291 (2016) 23047-23057.
- [12] Q.K. Tran, J. Leonard, D.J. Black, O.W. Nadeau, I.G. Boulatnikov, A. Persechini, J. Biol. Chem. 284 (2009) 11892-11899.
- [13] T.J. McCabe, D. Fulton, L.J. Roman, W.C. Sessa, J. Biol. Chem. 275 (2000) 6123-6128.
- [14] H. Zheng, J. He, J. Li, J. Yang, M.L. Kirk, L.J. Roman, C. Feng, JBIC J Biol Inorg Chem 24 (2019) 1-9.

- [15] N.L. Pirman, K.W. Barber, H.R. Aerni, N.J. Ma, A.D. Haimovich, S. Rogulina, F.J. Isaacs, J. Rinehart, Nat Commun 6 (2015) 8130.
- [16] J.E. Balke, L. Zhang, J.M. Percival, Nitric Oxide 82 (2019) 35-47.
- [17] F. Silvagno, H. Xia, D.S. Bredt, J. Biol. Chem. 271 (1996) 11204-11208.
- [18] C.J. Feng, L.J. Roman, J.T. Hazzard, D.K. Ghosh, G. Tollin, B.S.S. Masters, FEBS Lett. 582 (2008) 2768-2772.
- [19] H. Ihara, A. Kitamura, S. Kasamatsu, T. Ida, Y. Kakihana, H. Tsutsuki, T. Sawa, Y. Watanabe, T. Akaike, Biochem J 474 (2017) 1149-1162.
- [20] S. Kasamatsu, H. Tsutsuki, T. Ida, T. Sawa, Y. Watanabe, T. Akaike, H. Ihara, Nitric Oxide 120 (2022) 44-52.
- [21] K. Wada, K. Osuka, Y. Watanabe, N. Usuda, M. Fukasawa, Y. Araki, S. Okamoto, T. Wakabayashi, Nitric Oxide 81 (2018) 67-74.
- [22] K. Osuka, Y. Watanabe, N. Usuda, K. Atsuzawa, M. Takayasu, Neurochem. Int. 63 (2013) 269-274.
- [23] K. Mohler, J. Rinehart, in: B.A. Garcia (Ed.), Methods Enzymol., vol. 626, Academic Press, 2019, pp. 539-559.
- [24] S.P. Panda, W. Li, P. Venkatakrishnan, L. Chen, A.V. Astashkin, B.S.S. Masters, C. Feng, L.J. Roman, FEBS Lett. 587 (2013) 3973-3978.
- [25] H. Zheng, J.M. Weaver, C. Feng, J. Inorg. Biochem. 214 (2021) 111298.
- [26] F.A. Solari, M. Dell'Aica, A. Sickmann, R.P. Zahedi, Mol. Biosyst. 11 (2015) 1487-1493.
- [27] L.J.M. Dekker, L. Zeneyedpour, S. Snoeijers, J. Joore, S. Leenstra, T.M. Luider, J Proteome Res 17 (2018) 1654-1663.
- [28] S. Pou, L. Keaton, W. Surichamorn, G.M. Rosen, J Biol Chem 274 (1999) 9573-9580.
- [29] Y. Xia, A.L. Tsai, V. Berka, J.L. Zweier, J Biol Chem 273 (1998) 25804-25808.

- [30] J. Weaver, S. Porasuphatana, P. Tsai, S. Pou, L.J. Roman, G.M. Rosen, Biochimica Et Biophysica Acta-General Subjects 1726 (2005) 302-308.
- [31] H. Zhao, J. Joseph, H. Zhang, H. Karoui, B. Kalyanaraman, Free Radic Biol Med 31 (2001) 599-606.
- [32] E.S. Furfine, M.F. Harmon, J.E. Paith, R.G. Knowles, M. Salter, R.J. Kiff, C. Duffy, R. Hazelwood, J.A. Oplinger, E.P. Garvey, J Biol Chem 269 (1994) 26677-26683.
- [33] J. Vasquez-Vivar, B. Kalyanaraman, P. Martasek, N. Hogg, B.S. Masters, H. Karoui, P. Tordo, K.A. Pritchard, Jr., Proc Natl Acad Sci U S A 95 (1998) 9220-9225.
- [34] H. Yoneyama, A. Yamamoto, H. Kosaka, Biochem. J 360 (2001) 247-253.
- [35] Y. Xia, L.J. Roman, B.S.S. Masters, J.L. Zweier, J. Biol. Chem. 273 (1998) 22635-22639.
- [36] S. Adak, C. Crooks, Q. Wang, B.R. Crane, J.A. Tainer, E.D. Getzoff, D.J. Stuehr, J. Biol. Chem. 274 (1999) 26907-26911.
- [37] J. Tejero, L. Hannibal, A. Mustovich, D.J. Stuehr, J. Biol. Chem. 285 (2010) 27232-27240.
- [38] C. Cortes-Gonzalez, J. Barrera-Chimal, M. Ibarra-Sanchez, M. Gilbert, G. Gamba, A. Zentella, M.E. Flores, N.A. Bobadilla, Cell. Physiol. Biochem. 26 (2010) 657-668.
- [39] Y. Song, A.J. Cardounel, J.L. Zweier, Y. Xia, Biochemistry 41 (2002) 10616-10622.
- [40] E.D. Garcin, C.M. Bruns, S.J. Lloyd, D.J. Hosfield, M. Tiso, R. Gachhui, D.J. Stuehr, J.A. Tainer, E.D. Getzoff, J. Biol. Chem. 279 (2004) 37918-37927.
- [41] T. Jiang, G. Wan, H. Zhang, Y.P. Gyawali, E.S. Underbakke, C. Feng, Biochemistry 62 (2023) 2232-2237.
- [42] L.J. Roman, B.S.S. Masters, J. Biol. Chem. 281 (2006) 23111-23118.
- [43] S.A. Belambri, L. Rolas, H. Raad, M. Hurtado-Nedelec, P.M.-C. Dang, J. El-Benna, Eur J Clin Invest. 48 (2018) e12951.
- [44] J.R. Steinert, T. Chernova, I.D. Forsythe, The Neuroscientist 16 (2010) 435-452.
- [45] S. Araki, K. Osuka, T. Takata, Y. Tsuchiya, Y. Watanabe, Int J Mol Sci 21 (2020), 7997.

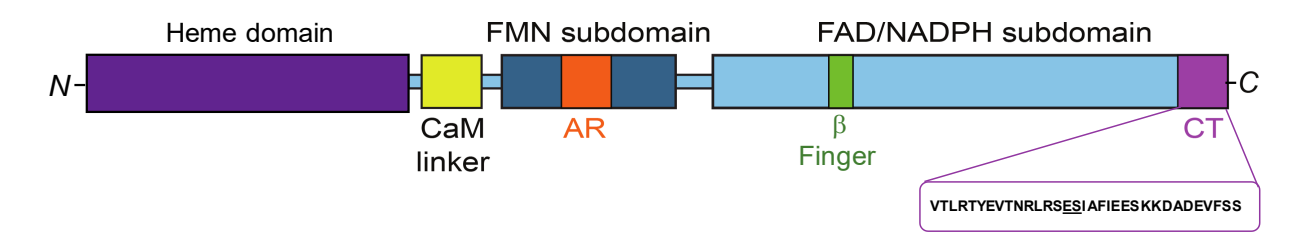


Figure 1. Domain organization of nNOS subunit. $nNOS\infty$ contains 34 additional amino acids in the AR region, compared to $nNOS\alpha$. The AR insert within the FMN subdomain and the CT function as CaM-responsive regulatory elements, inhibiting electron transfer out of the reductase domain when CaM is absent. CaM binds to the linker in between the FMN and heme domains and activates NO production by nNOS. This study investigates the phosphorylation at Ser1412 and Ser1446 within the CT region of nNOS variants α and ∞ , respectively; the serine site is underlined in the CT sequence.

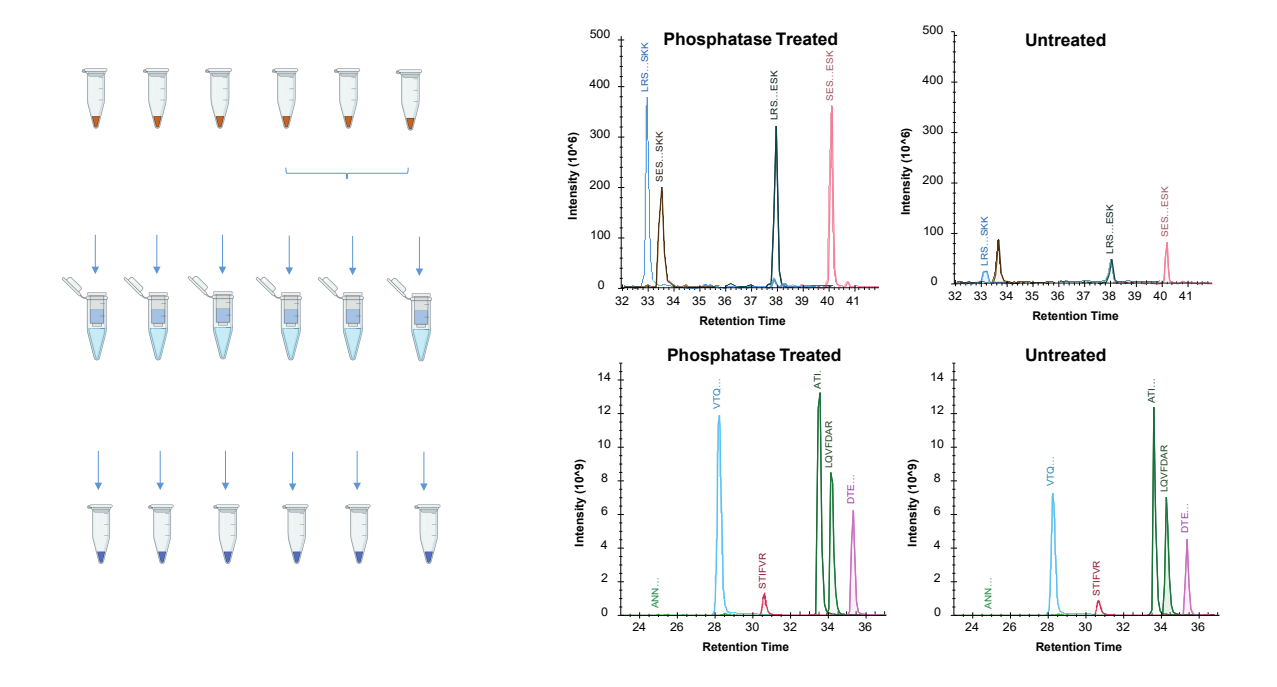


Figure 2. Phosphorylation stoichiometry determination of pSer1412 rat nNOSα by quantitative mass spectrometry. **A.** Sample preparation workflow prior to LC-MS/MS analysis. **B. Top:** PRM chromatogram of peptides containing 1412 site from the nNOSα protein with or without lambda phosphatase treatment; the scale of Y axis (intensity) was set as the same to illustrate the significantly higher intensities of unphosphorylated peptides in the phosphatase treated sample, showing high pSer%. **Bottom:** PRM chromatogram of six internal peptide references from the samples. Note that the internal reference peptides were selected for normalization purposes and that their intensities were similar in the treated and untreated samples. Similar internal reference peptide intensities demonstrate minimum sample loss during the experiments as the treated and untreated samples had the same amount of total nNOS protein to start with. The phosphorylation stoichiometry was calculated from intensities of unphosphorylated Ser1412 containing-peptides in the two differently treated samples, using the internal peptide references to normalize the intensities.

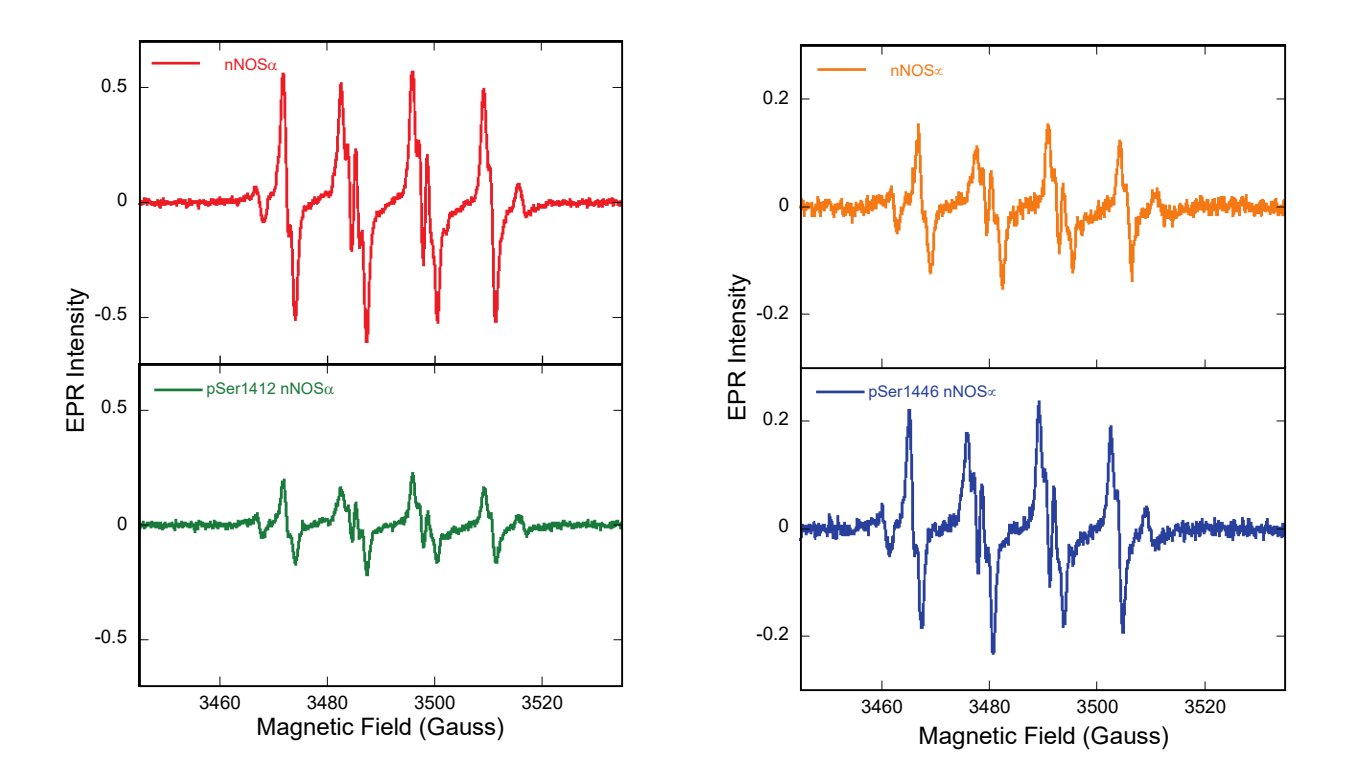


Figure 3. Superoxide (O_2^{\bullet}) production was assessed in the two nNOS splice variants, nNOSα (left panels) and nNOSα (right panels), under L-Arg depletion conditions; the Y axis scale differs between the left and right panels. Notably, in the unphosphorylated proteins, nNOSα exhibited a greater capacity to generate O_2^{\bullet} than nNOSα. Furthermore, pSer1446 nNOSα generated significantly more BMPO- $^{\bullet}$ OOH adduct than its unphosphorylated counterpart, while pSer1412 nNOSα demonstrated the opposite effect. These measurements were conducted in a phosphate buffer solution (50 mM, pH 7.4, with 0.1 mM EDTA and 0.1 mM DTPA) containing 20 nM nNOS, 1 αM CaM, 20 mM BMPO, and 0.5 mM CaCl₂. The reaction was initiated by adding NADPH (150 αM final concentration), and the EPR signals were collected 15 minutes after the mixing. The final concentrations of nNOS proteins were maintained at 20 nM in all these samples.

Table 1. Rates of NO synthesis and NADPH oxidation in the presence of 100 ${\rm \infty M}$ L-Arg $^{\rm a}$

	NO synthesis (min ⁻¹)	NADPH oxidation (min ⁻¹)	NADPH/NO
wild type nNOS∞	57.2 ± 2.8	122.2 ± 4.0	2.14 ± 0.07
pSer1446 nNOS∞	60.3 ± 1.8	124.2 ± 1.1	2.06 ± 0.06
wild type nNOSα	67.4 ± 6.9	139.3 ± 2.1	2.07 ± 0.21
pSer1412 nNOSα	64.5 ± 3.5	136.3 ± 1.1	2.11 ± 0.12

^a Rates are the average of at least three assays.